

# The Arm-Perturbator: Design of a Wearable Perturbation Device to measure Limb Impedance

Hannes Höppner, Dominic Lakatos, Holger Urbanek and Patrick van der Smagt  
DLR – German Aerospace Center  
Institute of Robotics and Mechatronics  
Wessling, Germany  
hannes.hoepfner@dlr.de, dominic.lakatos@dlr.de, holger.urbanek@dlr.de, smagt@dlr.de

**Abstract**—A method for and the design of a wearable system to measure mechanical impedance, e.g., to measure the stiffness of the human arm during natural movements, is described. With the new setup it will be possible to induce forces up to 1300 N within a timeframe of less than 25 ms using a defined impact rather than an oscillating force. The approach is compared to various existing solutions, showing the advantages of the new approach. A theoretical analysis of the approach is used for a simulation, in order to optimize the system parameters. Finally, measurements for verifying the simulation and identifying important influences on the system performance are described.

**Keywords**—Arm-Perturbator, arm movements, perturbation analysis, human limb impedance, stiffness measurements.

## I. INTRODUCTION

Measuring mechanical human arm properties such as stiffness and inertia, is not only important from a bio-mechanical point of view, but also from a robotic point of view. After all, recent developments in robotic systems have introduced actuation systems with variable stiffness, moving robotics away from the classical stiff approach towards flexible robots. This is a key characteristic for robots that are intended to act in an environment together with humans in order to be safe for both [1].

For this several elastic joints with variable stiffness have been developed at different research institutes in the past. One such robot example is being developed at DLR, the so called Hand-Arm-System HASy [2] (see Fig. 1). This system is designed to be similar to the human arm in its kinematic and dynamic properties, but also to be robust against unforeseen collisions. It consists of 26 joints, each having controllable position and stiffness parameters, thus summing up to 52 independent DoF (degrees of freedom). In HASy, different types of variable stiffness joint implementations are included, such as an antagonistic principle for the finger joints (as found in biology) [3], a so-called Bidirectional Antagonistic Variable Stiffness (BAVS) joint [4] and a Floating Spring Joint (FSJ) [5].

With HASy, a system will be available in which joint stiffness can be adjusted very similar to biology. This however raises the question of how such stiffness should be adjusted

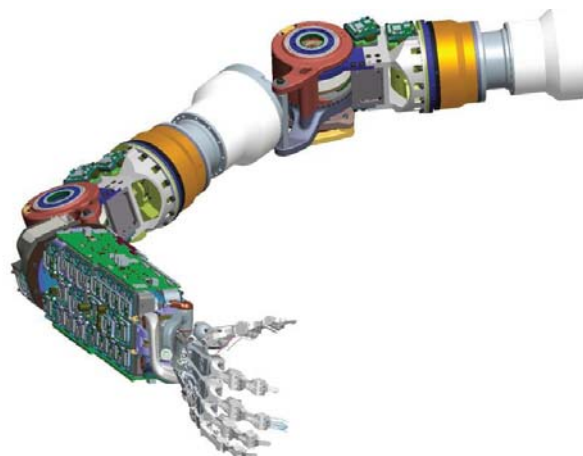


Fig. 1. Rendering of DLR Hand-Arm-System HASy [2].

optimally for the task at hand. Rather than attempting to analyse task-dependent stiffness optimisation theories from scratch, we prefer to look into human impedance and to extract rules from the found behaviour.

For this we plan to measure human limb impedance during various natural tasks, such as solving peg-in-hole problems, during catching, or other tasks involving physical interactions with the world around us. Many approaches towards measuring limb impedance have been proposed in the last 25 years. But nearly all of them measure the impedance by *position perturbation*, in which a robot-arm is fixed to the human arm and induces a positional disturbance. The main disadvantage of position perturbation-based methods is the dependence on a robotic system that is fixed to the world. This means that the test person is limited to moving in a very small workspace defined by the workspace of the robot along predefined trajectories, and that the complexity of the perturbing robot increases rapidly with the DoFs possible for the motion. Therefore many researchers only investigate planar movements (more details are given in section II).

In this paper we introduce a new measurement device using *force perturbation*, in which we expect to tackle the above-

mentioned problems. The advantage of the described device is its wearability, allowing the person to move around freely during the measurements, while being able to freely define limb trajectories without being impeded by the measuring device.

The data gathered from the human gives insight into human motor control with respect to limb impedance and offers the possibility to transfer this knowledge to variable-stiffness robotic systems through defined cost functions for task-dependent stiffness adjustment strategies.

The next section will give an overview of up-to-date used methods for measuring human limb impedance. After this we will define the specifications for a system that solves problems in current human impedance measurements. Next we will approach the new device from a theoretical point of view, including simulations of the device, followed by the description of the real hardware implementation. In the section "Measurements" we present measurements of the implementation, focussing on the influence of various parameters on the system performance. Finally, within "Discussions" we summarize the results and outline our future work.

## II. RELATED WORK

The idea of a wearable system for measuring human limb mechanical properties is not new. In 1986 Prof. J.E. Colgate, a former member of the group around Prof. Neville Hogan at Massachusetts Institute of Technology suggested in his Master Thesis [6] a so-called Dynamics Measuring Device (DMD). The DMD is using air pressure for a controlled disturbance of the arm. To that end, eight nozzles are aligned on a cuff that is fixed to the wearer's arm. The alignment of the eight nozzles allow to induce translational forces in all three Cartesian dimensions, four nozzles for the  $z$ -axis (distal, proximal), two for the  $y$ -axis (palmar, dorsal) and two for the  $x$ -axis (radial, ulnar). DMD is able to induce forces only and no torques due to being a prototype only. Work on the DMD seems to never have been carried on, however. The whole measuring device weights about 454 g and is able to induce forces up to approximately 5.33 N with a bandwidth of the controller of up to 8 Hz in all directions. The deflection of the arm is measured by an optical tracking system called TRACK, which uses two cameras to track the position of up to 30 infrared LEDs with a sampling rate of 315 Hz. By differentiating the positional information of the tracking system, velocity and acceleration are available in order to calculate the impedance of the joint. The perturbing force of the DMD is limited by the pressure that can be applied to the system regarding the system specification (15.2 bar). A pressure higher than 17.2 bar produces excessive noises and may cause harm to the ear.

Based on the DMD system other wearable systems have been developed. In [7] Xu *et al.* suggested a so-called Airjet Actuator System. This device is also based on force-perturbation, inducing a known force and measuring the deflection of the perturbed limb. The device uses compressed air as the power source to deflect the arm. For this the airjet uses two integrated fluidic spool valves to control the mass flow

and to switch the direction of the perturbation force using the so-called Coanda effect. With that setup it is possible to induce an oscillating perturbation to a test-person's arm with a frequency of up to 100 Hz. The deflection of the arm is measured by an optical tracking system named OPTOTRAK. Due to using air pressure as the power source and applying high frequencies the maximum force that can be exerted by the device is around 4 N [7]. Using this principle perturbation in all three Cartesian translational directions is possible, but the group, despite having built up a two-dimensional system [9], only reported on one-dimensional studies [10].

As mentioned before, the standard approach to measure limb stiffness is by position perturbation. Its measuring principle is inducing a known displacement and measuring the force exerted by the limb. Normally a rigid robotic actuator with high stiffness is used to which the test person is mechanically coupled, while said test person performs a predefined planar movement, starting from an initial position and getting perturbed randomly while trying to reach some target, e.g. as suggested in [11]. The force sensor is usually located at the coupling point between human arm and the robot.

## III. SPECIFICATION

The main disadvantage of these perturbation setups is the non-wearability of the perturbing device, and the fact that the test person only can do non-natural constrained movements. An important drawback of the abovementioned airjet actuator system and DMD system is that only forces up to 4 N and 5.33 N are realizable. Thus the influence of heavy loads during common tasks can not be identified clearly [10]. Furthermore, precise control of the device seems to be problematic, so that repeatability of the experiments cannot be guaranteed.

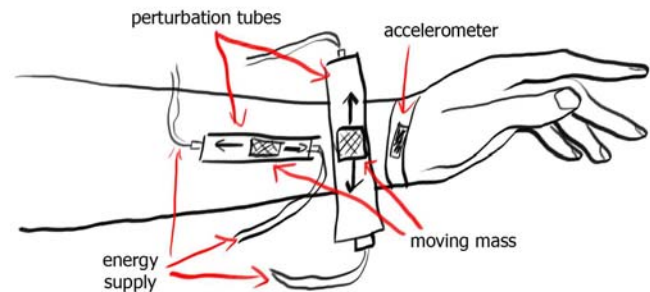


Fig. 2. Schematic diagram of the Arm-Perturbator.

To solve these issues we introduce a new device (see Fig. 2), based on force perturbation. For perturbing the arm, a mass is accelerated and decelerated inside a tube fixed to the limb. Energy is introduced using an external energy reservoir; in our case, we use compressed air. Both the acceleration phase, as well as the deceleration phase (the impact of the mass) induce a perturbation force to the limb.

We aim to investigate intrinsic muscle-tendon impedance, rather than investigate the effects of spino-cerebellar reflexes.

In order to exclude the influence of reflexes, we ensure that the Perturbator induces effects within the timespan of 25 ms, in accordance with latency of the reflex loop for shoulder muscles as found in [12, S.136]. For this we require the energy source to transfer enough mechanical energy within this timeframe. We decided to use compressed air instead of hydraulics as the power source, avoiding the risk of leakages and to increase its usability as compressed air is easy to transport and readily available, despite the fact that oil has a higher energy density while inducing lower delays. We excluded wearable electromagnetic-based actuators due to their insufficient force-to-weight ratio and bulkiness [7].

In order to realise oscillating perturbations as it is suggested in [7], multiple perturbations are needed within the 25 ms reflex delay time to be able to do a proper modal analysis. Using compressed air as power source, frequencies this high cannot be achieved since air is a compressible fluid, causing high delays. Another point to consider is that increasing frequency results into decreasing perturbation forces because of pneumatic delays. We therefore chose not to consider oscillating perturbations.

For inducing clear rotations and translations an alignment of the arm's distal axis and the perturbation axis is required. Using only one cylinder leads to fixing it in front of the arm as [7]. But due to allowing a perturbation of the supination and pronation at least two cylinders are necessary to induce pure translations or rotations (see Fig. 3). In order to perturb in six DoF's simultaneously at least six cylinders are necessary. However, we reduce the number of cylinders to two in order to keep the weight at a manageable amount.

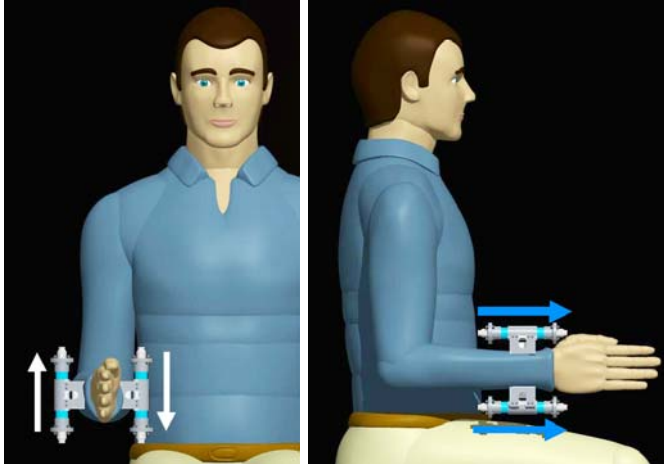


Fig. 3. Examples for different alignments of two Perturbators to induce pure translations or rotations.

Thus we can perturb a human in two DoFs simultaneously. To perturb the other four DoFs the alignment of the cylinders has to be changed. For measuring mechanical properties such as stiffness, we also have to measure arm displacement during perturbation. Because we are mainly interested in the impedance of the human arm's endpoint during various tasks

and because of small deflections we plan to measure arm deflections using an acceleration sensor with a sampling rate of up to 10 kHz. Additionally we measure the induced force at the coupling between the Perturbator and the human arm because this force is mainly depending on the impedance of the arm.

#### IV. THEORETICAL CONSIDERATIONS

The following section presents a simulation to estimate the system performance of the pneumatically driven Perturbator. The whole system can be seen as two separate models: a thermodynamical and a mechanical model which are connected via physical quantities.

##### A. Thermodynamical Sub-System

Fig. 4 shows the thermodynamical sub-system inside the dashed system boundaries, taken as an open system because mass flow  $\dot{m}$  is transported across the system boundaries. Additionally the system interchanges various kinds of energy such as heat  $P_W$  and work, and thus is neither rigid nor adiabatic.

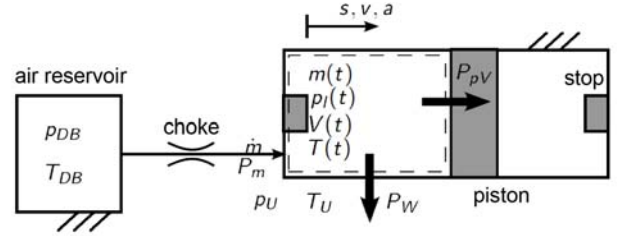


Fig. 4. Thermodynamical model of the perturbation tube.

The amount of transported energy through the system boundaries, according to the first law of thermodynamics is equal to the internal energy stored in the system. Neglecting the kinetic and potential energy of the gas we get

$$P_s = \dot{U} = P_m - P_{pV} - P_W, \quad (1)$$

where  $\dot{U}$  is the rate of change of the internal energy

$$\frac{dU}{dt} = m \cdot c \cdot \frac{dT}{dt}, \quad (2)$$

with  $m$  as the mass inside the system and  $c$  as the specific heat capacity.

$$P_m = R \cdot \dot{m} \cdot \begin{cases} T_{DB} & \text{if } \dot{m} > 0, \\ T & \text{if } \dot{m} \leq 0, \end{cases} \quad (3)$$

is the mass flow performance with  $R$  as the specific gas constant.  $P_m$  depends on the direction of the mass flow  $\dot{m}$ , either proportional to the temperature  $T$  in the considered system or proportional to the temperature  $T_{DB}$  in the pressure vessel. As usual in thermodynamics the energy that is added to the system has a positive and the dissipated energy a negative sign. Thus the pressure-volume-performance,

$$P_{pV} = p_l \cdot \frac{dV}{dt} = p_l \cdot \dot{V}, \quad (4)$$

had to be considered with a negative sign in Eq. (3), with  $p_l$  as the system pressure and  $\dot{V} > 0$  as an increase in volume. This means by moving the piston forward work is withdrawn from the thermodynamical system. The heat flow,

$$P_W = K_1 \cdot (T - T_U), \quad (5)$$

with  $K_1$  as the heat transfer coefficient considers the heat transported across the system boundaries and is thus a function of temperature difference  $T - T_U$  between the temperature of the system  $T$  and the ambient temperature  $T_U$ . Assuming that the working medium is an ideal gas,

$$p_l = \frac{m \cdot R \cdot T}{V}, \quad (6)$$

is the relation between the values of the Eq. (2)-(5). To calculate the mass flow the orifice formula for compressible media,

$$\dot{m} = A \cdot p_1 \cdot \sqrt{\frac{2}{R \cdot T_1}} \cdot \psi \cdot \zeta \cdot \alpha, \quad (7)$$

is used according to [13] where  $\zeta$  is the drag coefficient,  $\alpha$  the flow coefficient and  $\psi$  the flow function:

$$\psi = \begin{cases} \psi_{max} = 0.04841 & \text{supercritical flow,} \\ & \text{flow velocity = sonic velocity,} \\ \sqrt{1 - \left(\frac{p_2 - b}{p_1 - b}\right)^2} & \text{subcritical flow,} \\ & \text{flow velocity < sonic velocity,} \end{cases}$$

that takes into account the pressure ratio  $p_1$  before and  $p_2$  behind the choke. The values  $\alpha$  and  $\zeta$  consider the deviations from an ideal nozzle. Substituting the continuity equation

$$\dot{m} = Q \cdot \rho, \quad (8)$$

in Eq. (7) the orifice formula becomes

$$Q = \left( A \cdot \sqrt{\frac{2}{R \cdot T_1}} \cdot \frac{\zeta \cdot \alpha}{\rho} \right) \cdot \psi \cdot p_1. \quad (9)$$

Usually the manufacturers of pneumatic valves specify the nominal flow rate  $Q_N$  for an expansion from 7 bar to 6 bar. Thus the volume flow follows from the ratio

$$\begin{aligned} \frac{Q}{Q_N} &= \frac{\left( A \cdot \sqrt{\frac{2}{R \cdot T_1}} \cdot \frac{\zeta \cdot \alpha}{\rho} \right) \cdot \psi \cdot p_1}{\left( A \cdot \sqrt{\frac{2}{R \cdot T_1}} \cdot \frac{\zeta \cdot \alpha}{\rho_N} \right) \cdot \psi_N \cdot p_{1N}} = \\ &= \frac{\psi \cdot p_1}{\psi_N \cdot p_{1N}} \cdot \frac{\rho_N}{\rho}, \end{aligned} \quad (10)$$

so that the mass flow becomes

$$\dot{m} = \frac{\psi \cdot p_1}{\psi_N \cdot p_{1N}} \cdot Q_N \cdot \rho_N. \quad (11)$$

### B. Mechanical Sub-System

To calculate the pressure-volume performance by Eq. (4) the rate of volume change  $\dot{V} = A_K \cdot v$  and for calculating the heat flow by Eq. (5) the piston stroke  $s$  is required. Therefore a mechanical sub-system which is coupled with the thermodynamical model via these values is necessary (see Fig. 5).

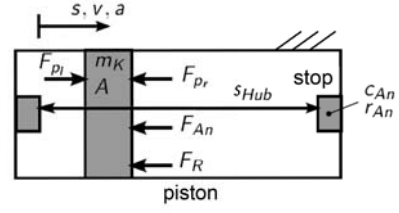


Fig. 5. Mechanical model of the perturbation tube.

From the centre-of-mass-theorem follows the differential equation of motion,

$$m_K \cdot a = F_{p_l} - F_{p_r} - F_R - F_{A_n}, \quad (12)$$

of the piston mass  $m_K$ . Here, the pressure acting on the piston surface from the left,

$$F_{p_l} = A \cdot p_l, \quad (13)$$

is proportional to the coupling value  $p_l$  of the thermodynamical sub-system. Analogous to the force acting on the left side of the mass the force acting on the right side is

$$F_{p_r} = A \cdot p_r, \quad (14)$$

and proportional to the ambient pressure  $p_U = p_r$ .

To determine the frictional force  $F_R$  a model proportional to velocity  $v$  is adopted,

$$F_R = k \cdot v, \quad (15)$$

where  $k$  is a friction-constant.

The force which acts on the stop  $F_{A_n}$  is modelled as a viscoelastic contact force and is defined by the piecewise continuous function

$$F_{A_n} = \begin{cases} c_{A_n} \cdot s + r_{A_n} \cdot v & \text{if } s \leq 0, \\ 0 & \text{if } 0 < s < s_{Hub}, \\ c_{A_n} \cdot (s - s_{Hub}) + r_{A_n} \cdot v & \text{if } s \geq s_{Hub}, \end{cases} \quad (16)$$

with the spring constant  $c_{A_n}$  and damping constant  $r_{A_n}$ .

### C. Simulation of the Perturbation Device

As mentioned before, the two sub-systems are coupled via the thermodynamical value system pressure  $p_l$  and the mechanical values piston stroke  $s$  and rate of volume change  $\dot{V}$ . With these two models a simulation of the perturbation device can be realized. Particularly the forces on the cylinder shell are of great interest whose sum,

$$F_S = F_R + F_{A_n} - (F_{p_l} - F_{p_r}) = -m_K \cdot a, \quad (17)$$

is equal to the shearing force between the Perturbator and the human arm. The model is simulated with the help of MATLAB-SIMULINK. Different parameters in Eq. (1)-(16) that define the specifications of the perturbation device have to be optimized. The goal of the optimization is to maximize the perturbation force  $F_S$  while ensuring that the measuring time—a full movement of the mass between the stops—is less than the human reflex time of 25 ms.

Another requirement is to minimize the weight. For the prototype we decided on a maximum weight of one tube of 500 g, because as mentioned before more mass means more constraints for the human and thus unwanted influence on the stiffness. The described simulation is mainly used to validate the parameters assumed in the construction of the prototype. In Fig. 6 the time course of the piston stroke, velocity and

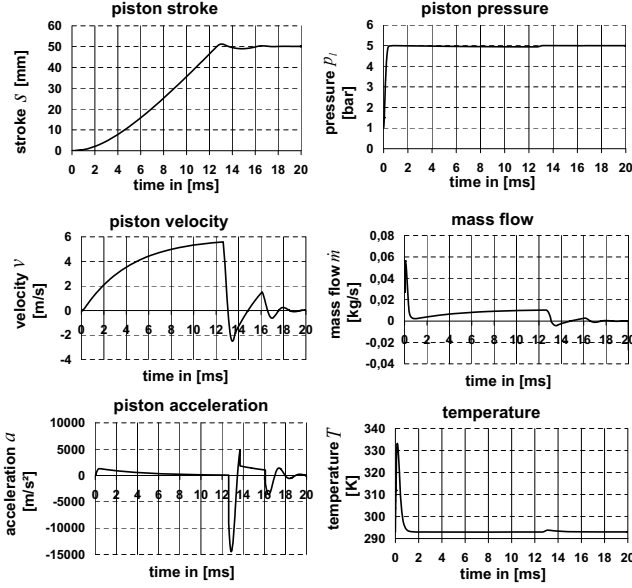


Fig. 6. Simulation of the perturbation tube.

acceleration after a leap in pressure at  $t = 0$  s is shown<sup>1</sup>.

Additionally the time course of the pressure, mass flow and temperature inside the tube is illustrated. Between  $0 < t < 2$  ms the piston moves only insignificantly and thus the volume is initially compressed. This compression causes an increase in temperature. However, once the piston begins to move, the

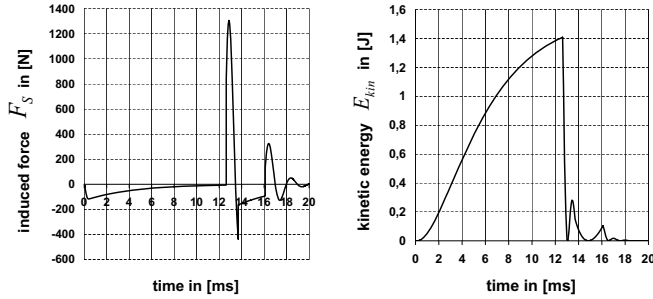


Fig. 7. Simulation of induced force  $F_S$  and kinetic energy  $E_{kin}$ .

volume of air inside the cylinder is able to expand and the temperature decreases back to ambient. Because the pressure is limited to 5 bar and the friction force increases with an increase of velocity (see Eq. (15)) the acceleration starts decreasing.

<sup>1</sup>The parameters used for the simulation are:  $c_{An} = 1e6$  N/m,  $d_{An} = 150$  kg/s,  $s_{Hub} = 50$  mm,  $p_l = 5$  bar,  $m_K = 0.0902$  kg,  $d = 20$  mm,  $k = 21$  (N · s)/m,  $K_1 = 100$  (N · m)/(s · K).

Fig. 6 shows that the whole measurement time is below 16 ms and thus below the required 25 ms. The abrupt deceleration of the piston when reaching the stop between  $12$  ms  $< t < 20$  ms is obvious in piston stroke, velocity and acceleration as well as in the thermodynamic state variables.

Integrating the force acting on the cylinder shell supplies the impulse,

$$p = \int F_S(t)dt = m_K \int \ddot{s}(t)dt = m_K \cdot v(t), \quad (18)$$

that is proportional to the velocity  $v$  of the piston. Having the impulse, the kinetic energy of the mass can be calculated easily:

$$E_{kin}(t) = \frac{p^2}{2 \cdot m_K} = \frac{1}{2} \cdot m_K \cdot v^2. \quad (19)$$

The simulated force acting on the cylinder shell  $F_S$  and the kinetic energy  $E_{kin}$  are shown in Fig. 7. The acceleration and deceleration of the mass can be clearly seen in both graphs. The maximum force induced at impact is about 1300 N. The graph of the kinetic energy shows that the essential part of the kinetic energy is transferred to the human arm before the mass reaches the stop at 16 ms. So future measurements on the human arm will show what part of the graph will be used to identify the impedance. The reaction of the arm to the induced force is not part of this paper.

## V. IMPLEMENTATION

With the specifications and the optimized parameters of the simulation a Perturbator<sup>2</sup> has been constructed as shown in Fig. 8. The centre is a steel cylinder of about 130 mm length

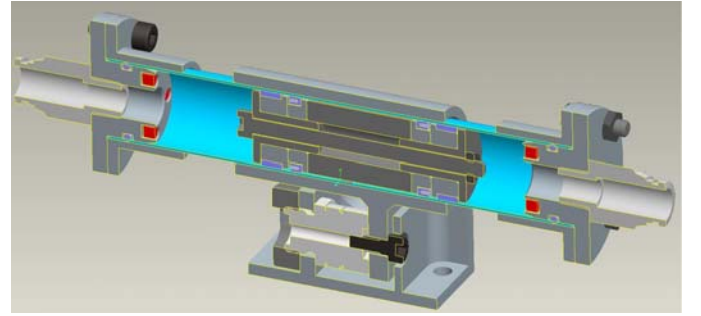


Fig. 8. Sectional view of the Arm-Perturbator.

with a high surface accuracy and a low wall thickness in order to reduce the total mass of the system and the friction between the cylinder and the piston. The piston itself consists of three functional elements: a mass that can be replaced by mass pieces with the same size but different density, and sealing elements and guiding surfaces to ensure high impermeability and low friction. Additionally magnets can be added at both stops (see the red cylinders in the sectional view in Fig. 8). The idea of the magnets is to increase the counterforce against the air pressure at the beginning before the mass begins to move in the case of too low friction force. The magnets were not

<sup>2</sup>Patent pending.

considered in the simulation. Between the basis which is fixed to the human arm and the steel cylinder a 1-DoF force sensor is mounted. The cylinder is guided on the basis using linear bearings in order to connect the cylinder, the sensor and the human arm in series. The advantage of this device is that it can be actuated bidirectionally, therefore allowing 2-DoF actuation with two actuators, viz. one translation and one rotation (see Fig. 3).

## VI. MEASUREMENTS

In Fig. 9 the finished Perturbator is shown. Because it can be driven bidirectionally two switchable electromagnetic valves are necessary, one to apply the pressure of the air reservoir and the other the ambient pressure, respectively. In the setup,



Fig. 9. Finished Perturbator after assembling.

we fixed the Perturbator to a base frame in order to measure actuation time and exerted force; magnets to increase the counterforce as mentioned in section V where not used during the whole measurement. In Fig. 10 the measured and simulated

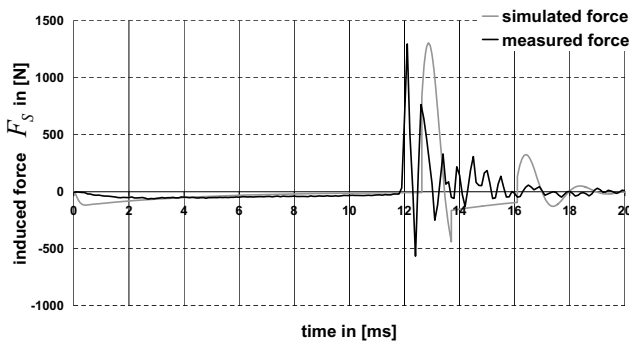


Fig. 10. Comparison between simulated and measured force  $F_S$ .

graph of the shell force is shown. A good correspondence between simulated and measured data is clearly visible. However, we see that the mass starts moving earlier in the measured graph than in the simulated graph. Furthermore, the time between both stops is lower in the measurements than in the simulation. This can be attributed to a lower friction force than

expected between the piston with the special guiding elements and the steel cylinder. Furthermore, it is obvious that the initial

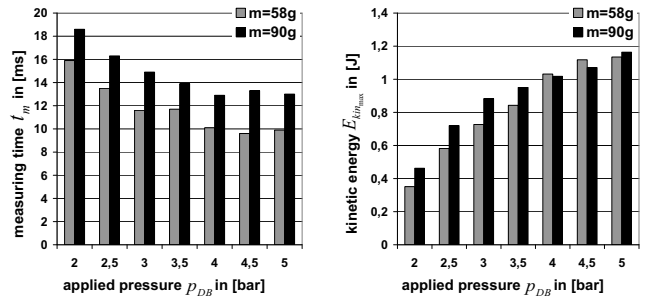


Fig. 11. Influence of the mass  $m_K$  and the applied air pressure  $p_{DB}$  to the measuring time  $t_m$  and maximum kinetic energy  $E_{kin}$ .

force acting on the cylinder shell and thus the acceleration is higher for the simulated graph. An explanation can be a difference in assumed and measured friction force for low and high velocities and a difference in the amounts of an ideal and real air reservoir. Another goal of the measurements is to figure

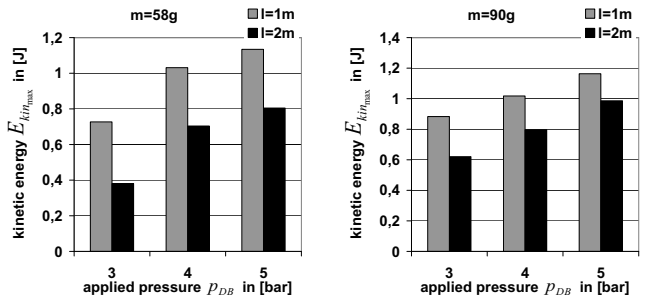


Fig. 12. Influence of the flexible tube length  $l$  to the induced kinetic energy  $E_{kin}$  for different masses.

out the influence of the piston mass, of the applied pressure and of the flexible tube length to the measuring time and the induced kinetic energy. In Fig. 11 the influence of the mass and

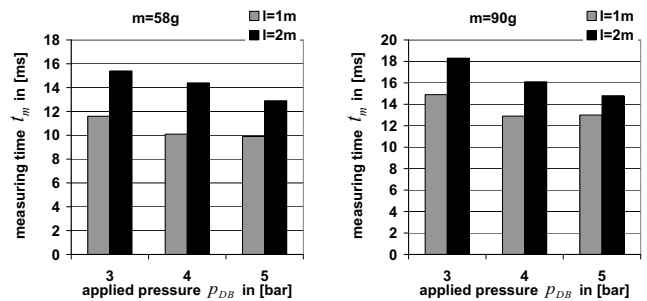


Fig. 13. Influence of the flexible tube length  $l$  to the total measuring time  $t_m$  for different masses.

the applied pressure to the kinetic energy and the measuring time is shown, where the kinetic energy is the maximum of energy that is applied to the shell when reaching the impact. The figures show that increasing the applied pressure causes

decreasing of the measuring time and increasing of the induced kinetic energy. Thus increasing the applied pressure within the system limits has a positive effect to the system performance. On the other hand an increase in piston mass leads to a higher measuring time for all applied pressure levels. Furthermore increasing the piston mass results in a higher kinetic energy for pressures less than 4 bar, above it the kinetic energies are almost the same. This is caused by a quadratical influence of velocity and thus of applied pressure and a linear influence of mass to the kinetic energy. Additionally we measured the influence of the flexible tube length on the measuring time and the kinetic energy. As expected, increasing the flexible tube length—in this case from 1 m to 2 m—causes a higher measuring time and a lower induced kinetic energy and thus a worse system performance.

## VII. DISCUSSION

In this paper we presented a novel perturbation device for measuring human arm stiffness in unconstrained movement scenarios. This device involves moving a mass along a line, actuated via compressed air. As shown, the real system behaves as predicted by the simulation. A lower mass size, a high pressure and a low flexible tube length will lead to a better system performance. Substantial disturbances of over 1300 N well below the 25 ms human reaction time are possible, which will allow us to measure human limb impedance without measuring reflex influences.

However we have not yet conducted human experiments. The next step on the path will be to attach the Arm-Perturbator to some test-bed with adjustable impedance, like one of our robotic variable-stiffness joints. That gives a efficient opportunity to validate the stiffness—and perhaps even damping and inertia—data gained by the perturbation device.

One open issue still is an optimal connection between the device and the perturbed limb. This connection has to be able to optimally transfer the impacts of the Perturbator while at the same time it has to be comfortable to the test person, to be as unobstructive as possible.

Furthermore we will work on reducing the weight of the Perturbator, as it will decrease the load on the human arm. The more load the human arm has to carry, the more active the muscles are, and this may reduce the variance of possible stiffness the human can produce.

## ACKNOWLEDGEMENT

This work has been partially funded by the European Commission's Seventh Framework Programme as part of the project STIFF under grant no. 231576.

## REFERENCES

- [1] Sami Haddadin, Tim Laue, Udo Frese, Sebastian Wolf, Alin Albu-Schaeffer and Gerd Hirzinger, *Kick it with Elasticity: Safety and Performance in Human-Robot Soccer*, in: Robotics and Autonomous System - Special Issue on Humanoid Soccer Robots 2009
- [2] Markus Grebenstein and Alin Albu-Schäffer and Thomas Bahls and Maxime Chalon and Oliver Eiberger and Werner Friedl and Robin Gruber and Ulrich Hagn and Robert Haslinger and Hannes Höppner and Stefan Jörg and Matthias Nickl and Alexander Nothhelfer and Florian Petit and Benedikt Pleintinger and Joseph Reil and Nikolaus Seitz and Thomas Wimböck and Sebastian Wolf and Tilo Wüsthoff and Gerd Hirzinger, *The DLR Hand Arm System*, Submitted to ICRA 11
- [3] Markus Grebenstein and Patrick van der Smagt, *Antagonism for a highly anthropomorphic hand-arm system*, in: Advanced Robotics, 2008
- [4] F. Petit, M. Chalon, W. Friedl, M. Grebenstein, A. Albu-Schäffer, and G. Hirzinger, *Bidirectional antagonistic variable stiffness actuation: Analysis, design & implementation*, in Proc. IEEE Int Robotics and Automation (ICRA) Conf, 2010, pp.4189-4196
- [5] S. Wolf, O. Eiberger, and G. Hirzinger, *The DLR FSJ: Energy based design of a variable stiffness joint*, Submitted to ICRA 11
- [6] John Edward Colgate, *The Design of a Dynamics Measuring Device*, M.S. Thesis, Massachusetts Institute of Technology, Department Mechanical Engineering, January 1986
- [7] Yangming Xu, Ian W. Hunter, John M. Hollerbach and David J. Bennett, *An Airjet Actuator System for Identification of the Human Arm Joint Mechanical Properties*, in: IEEE Transactions on Biomedical Engineering, Vol. 38, No. 11, November 1991
- [8] Yangming Xu and John M. Hollerbach, *A Robust Ensemble Data Method for identification of Human Joint Mechanical Properties During Movement*, in: IEEE Transactions on Biomedical Engineering, Vol. 46, No. 4, April 1999
- [9] Yangming Xu and John M. Hollerbach, *Design and Calibration of a 2D Airjet Device for Human Motor Control Study*, in: Proc. 17th Annu. Conf. IEEE Eng. in Medicine and Biol. Soc., (September 1995)
- [10] Ana Maria Acosta, Robert F. Kirsch, Eric J. Perreault, *A robotic manipulator for the characterization of two-dimensional dynamic stiffness using stochastic displacement perturbations*, in: Journal of Neuroscience Methods 102, July 2000
- [11] David W. Franklin and Theodore E. Milner, *Adaptive control stiffness to stabilize hand position with large loads*, in: Exp Brain Res 152:211-220, Springer Verlag 2003
- [12] Herman van der Kooij, Bart Koopman, Frans C. T. van der Helm, *Human Motion Control*, Reader for Delft University course wb2407 and Twente University course 115047, January 2008 in: Exp Brain Res 152:211-220, Springer Verlag 2003
- [13] Holger Watter, *Hydraulik und Pneumatik. Grundlagen und Übungen - Anwendung und Simulation*, , ISBN 3834801909, publishing company: Vieweg Teubner, Spetember 2007